ABSENCE OF LOCALISATION IN OCEAN WAVE INTERACTIONS WITH A ROUGH SEABED IN INTERMEDIATE WATER DEPTH

by L. G. BENNETTS

(*School of Mathematical Sciences, University of Adelaide, Adelaide 5005, Australia*)

M. A. PETER

(*Institute of Mathematics, University of Augsburg, 86135 Augsburg, Germany and Augsburg Centre for Innovative Technologies, 86135 Augsburg, Germany*)

and H. CHUNG

(*School of Computer and Mathematical Sciences, Auckland University of Technology, Auckland PO Box 92006, New Zealand*)

[Received ?? ?? ????. Revise ?? ?? ????]

Summary

The possibility of a rough seabed causing localisation of ocean waves in intermediate water depth is considered. A numerical and analytical study of the localisation phenomenon is conducted using a transect model and linear potential theory. It is shown that although the effective wave field is strongly attenuated by the roughness, leading to previous predictions of localisation, individual wave fields are not localised.

1. Introduction

In many branches of wave science, a rough, i.e. randomly disordered, medium of sufficient length inhibits propagation of wave energy. The waves are thus localised in space. Localisation is a product of wave scattering. It is, therefore, a linear and conservative phenomenon. In the case of a steady monochromatic incident wave train, localisation is manifest as exponential attenuation of wave energy with distance travelled through the rough medium. (Wave fields can also display spots of relatively high intensity, known as speckle patterns.) The present investigation focusses on the mean attenuation rate with respect to many realisations of the rough medium, which, here, is open water over a rough seabed.

Belzons et al. [1] used wave tank experiments to show that shallow-water waves are localised by random steps in the tank floor in a one-dimensional setting. Devillard et al. [2] constructed an associated numerical model, based on linear shallow-water and full potential theories. They showed the localisation length, i.e. wave penetration distance, is proportional to the reciprocal of wave frequency squared in the asymptotic limit of large wavelengths, and tends to infinity for small wavelengths, i.e. localisation becomes very weak. (Both shallow-water and full potential theories predict the former property, whereas, only full potential theory predicts the latter, as shallow-water theory is not valid for small wavelengths.) Scaling arguments were used to predict that ocean waves would, similarly, be localised

by a rough seabed in shallow water. Guazzelli et al. [3] earlier predicted localisation of shallow-water waves by random spatial tank-floor/seabed fluctuations.

Subsequently, a series of numerical and theoretical studies of shallow-water-wave localisation have been conducted, based on potential theory or shallow-water theory. The broad motivations for the studies are to understand the role of localisation in (i) tsunami-wave hydrodynamics, and (ii) coastal protection provided by ocean wave/seabed interactions.

Nachbin and Papanicolaou [4] and Nachbin [5] developed theoretical predictions of localisation lengths of linear waves in two-dimensional transects, i.e. one-dimensional waves. The predictions were based on potential theory in the asymptotic limit of long waves in relation to the fluid depth (shallow water) and the characteristic length of the roughness, i.e. rapid fluctuations. Numerical solutions of the full-linear water-wave equations were used to validate the theory. Nachbin [5] also compared his localisation-length predictions to those of Devillard et al. [2], and showed that, consistent with the model of Devillard et al. [2] for large wavelengths, the localisation length is proportional to the reciprocal of wave frequency squared.

Nachbin and Sølna [6] studied the related problem of apparent diffusion of a pulse, induced by a rough seabed. They derived theoretical predictions of the effective, i.e. mean, pulse from statistical properties of the roughness, based on the linear shallow-water equations, in the small-amplitude-roughness limit. Further, they showed the effective pulse approximates individual pulses accurately. Numerical solutions of the nonlinear shallow-water equations were used to validate the theory and to show nonlinearitity is not a first-order effect for small-amplitude pulses.

Grataloup and Mei [7], Mei and Li [8] and Craig et al. [9] developed asymptotic theories for nonlinear shallow-water problems, assuming small wave amplitudes and small-amplitude bed roughness. Craig et al. [9] used potential theory, and, as with the linear studies referenced above, focussed on rapid seabed fluctuations. They showed diffusion is a property of the effective wave field, and is a high-order effect for individual wave fields, although they considered smaller amplitude roughness than Nachbin and Sølna [6].

Grataloup and Mei [7] and Mei and Li [8] based their theory on the Boussinesq equations, and used a continuous function to model the rough seabed, which was not restricted to rapid fluctuations. Grataloup and Mei [7] studied localisation of a simple harmonic incident wave train, and its impact on harmonic generation. Mei and Li [8] studied soliton evolution, and showed the spatial attenuation rate is algebraic in this case.

Pelinovsky et al. [10] studied localisation of linear water waves without the shallow-water or transect restrictions. They applied the Berkhoff approximation (mild bed slopes) to obtain predictions of localisation lengths of effective wave fields. Comparisons with the effective components of full-linear solutions revealed the approximation to be accurate in shallow-water and mild-bed-slope limits.

Stepaniants [11] used the Born approximation (weak scattering) to predict localisation lengths for waves in two-dimensional transects, with small-amplitude bed roughness. He compared the predictions with the shallow-water measurements of Belzons et al. [1] and model predictions of Devillard et al. [2]. He also noted his localisation-length predictions coincide with those of Nachbin [5] for large wavelengths. Further, he quantified the impact of localisation on ocean waves in the presence of viscous damping and currents.

In contrast to the investigations referenced above, here we are concerned with the regime

in which wavelengths are comparable to the water depth (intermediate water depth) and characteristic length of the roughness. Bed fluctuations generally cause weaker scattering in the intermediate-water-depth regime than the shallow-water regime. However, Mei and Hancock [12] predicted a small-amplitude rough seabed would localise weakly nonlinear ocean waves in intermediate water depths, and, hence, produce an effective dissipation of wave energy over long distances. The prediction was based on an approximate solution of a transect model, in which potential theory governs motions. Specifically, Mei and Hancock [12] employed a multiple-scale approximation to derive a closed form expression for the attenuation rate of the wave elevation, and hence the localisation length. The multiple-scale method is similar to that of Kawahara [13].

Pihl et al. [14] extended the transect model of Mei and Hancock [12] to three spatial dimensions, at the expense of having to use numerical methods to solve the nonlinear Schrödinger equation derived via the multiple-scale approximation. They showed the third dimension reduces attenuation rates. Luz and Nachbin [15] extended the theory of Mei and Hancock [12] to large-amplitude bed roughness. They showed the large amplitudes affect the stability of Stokes waves. Li and Mei [16] predicted localisation of internal gravity waves in a stratified ocean by a rough seabed, using a multiple-scale method analogous to that of Mei and Hancock [12].

We revisit the question of whether a small-amplitude rough seabed localises ocean waves in intermediate water depth, originally predicted by Mei and Hancock [12]. We focus on the validity of using the effective wave elevation to predict localisation of the individual (physical) wave elevations. For this purpose, attention is restricted to the canonical, linear version of the problem studied by Mei and Hancock [12], as outlined in § 7.4 of Mei et al. [17], and noting the theory of Mei and Hancock [12] predicts the linear and weakly nonlinear models provide identical attenuation rates.

We extract attenuation rates from large ensembles of numerical solutions of waves in long transects with rough seabeds, where the rough seabeds are randomly generated from distributions with prescribed root-mean-square amplitudes and characteristic lengths. We show attenuation rates of effective wave elevations far exceed those of the corresponding individual wave elevations, due to wave cancellation in the averaging process. The individual wave elevations do not, in general, attenuate rapidly enough to cause localisation of ocean waves due to a rough seabed.

Further, we extend the multiple-scale approximation of Mei et al. [17] to account for random components of individual wave fields at leading order. We thereby show the multiple-scale approximation captures the attenuation rate of the effective wave elevation, rather than the envelope of the full wave elevation. We also use our numerical solutions to determine regimes of validity of the multiple-scale approximation.

In the field of seismic waves, Wu [18] noted, similarly to us, that the attenuation rate of individual wave fields cannot be extracted from the effective wave field. He considered the regime in which wavelengths are much smaller than the characteristic length of the inhomogeneity in the medium. He used a one-dimensional model and neglected fluctuations in wave amplitude to show the attenuation of the effective wave field is a statistical effect produced by phase decoherence between ensemble members. Shapiro and Kneib [19] later showed attenuation of the effective wave field is also due to amplitude fluctuations. We are not aware of the issue of attenuation rates of individual wave fields versus effective wave fields being highlighted in other branches of wave science.

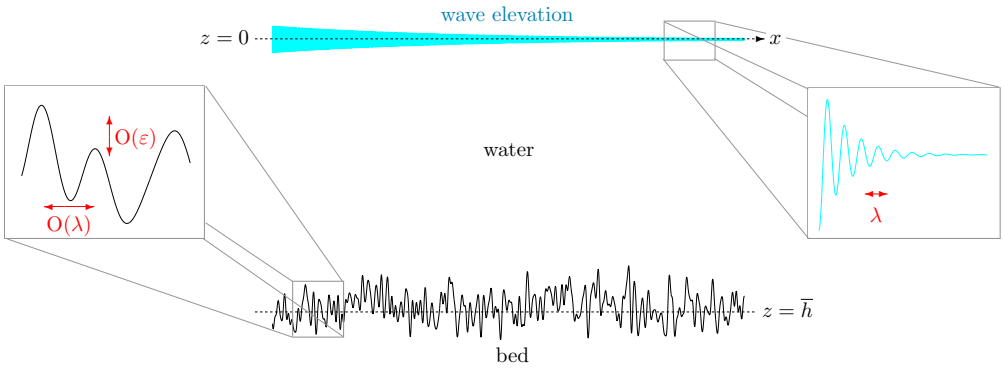

Fig. 1 Schematic of the geometry. Note that the aspect ratio exaggerates the vertical scale.

2. Preliminaries

Let spatial locations in a long transect (vertical cross-section) of the ocean be defined by the Cartesian coordinate system (x, z). Horizontal locations are defined by the coordinate x. Vertical locations are defined by the coordinate z. The vertical coordinate points upwards and has its origin set to coincide with the equilibrium position of the ocean surface.

Consider a monochromatic wave propagating in the positive x-direction. The wave amplitude is assumed to be sufficiently small with respect to the wavelength, λ, that linear theory is applicable. The wavenumber, $k = 2\pi/\lambda$, is related to the angular frequency, ω, via the dispersion relation

$$k \tanh(kh) = K \qquad \text{where} \qquad K = \omega^2/g. \tag{2.1}$$

Here h denotes the undisturbed fluid depth and $g \approx 9.81\,\mathrm{m\,s^{-2}}$ denotes acceleration due to gravity.

The seabed fluctuates about the mean depth $\bar{h}$. The fluctuations have a known characteristic length, l, and root-mean-square amplitude, ε, also referred to as the bed amplitude. The characteristic length is assumed to be comparable to the wavelength, i.e. $kl = \mathrm{O}(1)$. The root-mean-square amplitude is assumed small in relation to the wavelength, i.e. $k\varepsilon \ll 1$. The function $z = -h(x)$, where $h(x) = \bar{h} - \varepsilon\beta(x)$ and $\beta = \mathrm{O}(1)$, is used to denote the location of the bed. Fig. 1 shows an example geometry.

Under the usual assumptions of linear, time-harmonic wave theory, the velocity field of water particles in the ocean is defined as the gradient of $\mathrm{Re}\{(g/\mathrm{i}\omega)\phi(x,z)\mathrm{e}^{-\mathrm{i}\omega t}\}$, where Re denotes the real part of the included quantity. The (complex-valued) velocity potential, ϕ, satisfies Laplace's equation in the undisturbed fluid domain, i.e.

$$\partial_x^2\phi + \partial_z^2\phi = 0 \quad \text{in} \quad \Omega_h = \{x, z : x \in \mathbb{R} \ \text{ and } \ -h(x) < z < 0\}, \tag{2.2a}$$

where $\partial_x = \partial/\partial x$ and $\partial_z = \partial/\partial z$. An impermeability condition is applied on the seabed, i.e.

$$\partial_z\phi + h'(\partial_x\phi) = 0 \quad \text{on} \quad z = -h(x). \tag{2.2b}$$

The velocity potential is coupled to the wave elevation, denoted $z = \mathrm{Re}\{\eta(x)\mathrm{e}^{-\mathrm{i}\omega t}\}$, via

free-surface conditions applied at the equilibrium ocean surface. The free-surface conditions consist of a dynamic and a kinematic condition, and are, respectively,

$$\phi = \eta \quad \text{and} \quad \partial_z \phi = K\eta \quad \text{on} \quad z = 0, \tag{2.2c}$$

which are combined into the single condition $\partial_z \phi = K\phi$ $(z = 0)$ for the velocity potential.

3. Numerical simulations

3.1 *Step approximation and ensemble averaging*

Consider the problem in which the roughness extends over a long, finite interval $x \in (0, L)$. (We assume the interval is sufficiently long that the boundaries do not affect attenuation rates.) The bed is otherwise flat and extends to infinity in both positive and negative horizontal directions. A unit-amplitude incident wave is prescribed at $x \to -\infty$. The incident wave is defined by the velocity potential

$$\phi = \mathrm{e}^{\mathrm{i}kx} w(z) \qquad \text{where} \quad w(z) = \cosh\{k(z+h)\}/\cosh(kh). \tag{3.1}$$

We seek the resulting wave elevation in the interval containing the rough bed.

Let the rough bed profile, $h(x)$ $(0 < x < L)$, be approximated by a piece-wise constant function — the so-called step approximation. We use a piece-wise constant function with equal length sub-intervals. The sub-intervals are denoted (x_{m-1}, x_m) for $m = 0, \ldots, M+1$, with $x_0 = 0$ and $x_M = L$. The zeroth and $(M+1)$th sub-intervals denote the semi-infinite flat-bed intervals, i.e. $x_{-1} = -\infty$ and $x_{M+1} = \infty$. We denote the value of the function in the mth sub-interval as h_m, and set it to be equal to the value of the continuous bed profile at the mid-point.

We approximate the wave field in each sub-interval as a combination of the rightward- and leftward-travelling waves supported by the particular fluid depth. The approximation is motivated by the small bed amplitude. It can be extended to capture the full-linear solution by including evanescent wave components of the wave field. However, we verified numerically that evanescent wave components do not significantly affect our results. Numerical results presented in Sections 4 to 5, therefore, accurately represent full-linear solutions.

The velocity potential in the mth sub-interval is

$$\phi(x, z) = \left(a_m \mathrm{e}^{\mathrm{i}k_m x} + b_m \mathrm{e}^{-\mathrm{i}k_m x}\right) w_m(z) \quad \text{for} \quad x_{m-1} < x < x_m, \tag{3.2}$$

where k_m is the wavenumber for depth h_m and w_m is the corresponding vertical mode. The quantities a_m and b_m are, as yet, unknown (complex-valued) wave amplitudes. Incident wave forcing from $x \to -\infty$ only is set via $a_0 = 1$ and $b_{M+1} = 0$.

Wave fields in adjacent sub-intervals are related to one another at the interface between the sub-intervals via continuities of water pressure and horizontal velocity throughout the fluid column, i.e.

$$\phi(x_{m-}, z) = \phi(x_{m+}, z) \quad \text{and} \quad \frac{\partial \phi(x_{m-}, z)}{\partial x} = \frac{\partial \phi(x_{m+}, z)}{\partial x} \quad \text{for} \quad -h_m < z < 0, \tag{3.3}$$

and for $m = 0, \ldots, M$. The continuities are enforced in the weak sense, using the vertical

mode, $w(z)$, as the test function, i.e.

$$\int_{-h_{\widehat{m}}}^{0} \phi(x_{m-},z)w_{\widehat{m}}(z)\,\mathrm{d}z = \int_{-h_{\widehat{m}}}^{0} \phi(x_{m+},z)w_{\widehat{m}}(z)\,\mathrm{d}z \tag{3.4a}$$

$$\text{and} \qquad \int_{-h_{\widehat{m}}}^{0} \frac{\partial\phi(x_{m-},z)}{\partial x}w_{m-1}(z)\,\mathrm{d}z = \int_{-h_{\widehat{m}}}^{0} \frac{\partial\phi(x_{m+},z)}{\partial x}w_{m}(z)\,\mathrm{d}z, \tag{3.4b}$$

for $m = 0,\ldots,M$, where $\widehat{m} = m-1$ if $h_{m-1} < h_m$ and m otherwise. The continuity conditions reduce to scattering relations between wave amplitudes in adjacent sub-intervals. The relations are denoted

$$b_m = R_m^{(-)}a_m + T_m^{(+)}b_{m+1} \quad \text{and} \quad a_{m+1} = T_m^{(-)}a_m + R_m^{(+)}b_{m+1} \quad (m = 0,\ldots,M), \tag{3.5}$$

where $R_m^{(\pm)}$ and $T_m^{(\pm)}$ are, respectively, reflection and transmission coefficients for the mth step in isolation. They are considered to be known.

An iterative algorithm is chosen to calculate the amplitudes a_m $(m = 1,\ldots,M+1)$ and b_m $(m = 0,\ldots,M)$ from (3.5). Bennetts and Squire [20] give full details of the algorithm. The wave elevation, η, is subsequently recovered via the first component of equation (2.2c), to be

$$\eta(x) = a_m\mathrm{e}^{\mathrm{i}k_m x} + b_m\mathrm{e}^{-\mathrm{i}k_m x} \quad (x_{m-1} < x < x_m) \quad \text{for} \quad m = 0,\ldots,M+1. \tag{3.6}$$

Wave elevations are calculated for a large ensemble of randomly generated realisations of the bed profile. The bed profiles share the same amplitude, ε, and characteristic length, l. The relationship between the ensemble of bed profiles is expressed via the autocorrelation condition

$$\langle\beta(x)\beta(x-\xi)\rangle = \gamma(|\xi|), \tag{3.7}$$

where $\langle\cdot\rangle$ denotes the ensemble average of the included quantity with respect to realisations. We prescribe the Gaussian autocorrelation function $\gamma(\xi) = \mathrm{e}^{-\xi^2/l^2}$ for the remainder of our investigation, noting Mei and Hancock [12] showed an exponential autocorrelation function gives almost identical results. The characteristic length, l, is hence referred to as the correlation length from here on.

Two measures of the exponential attenuation rate are obtained from the ensemble of wave elevations. First, an attenuation rate, $Q_{\mathrm{eff}}^{(\mathrm{rs})}$, is extracted from the effective wave elevation, $\langle\eta\rangle$. The attenuation rate, in this case, is defined via

$$|\langle\eta\rangle| \approx \mathrm{e}^{-Q_{\mathrm{eff}}^{(\mathrm{rs})}x} \qquad (0 < x < L). \tag{3.8}$$

It is calculated using a least-squares minimisation routine. Second, an attenuation rate, $Q_{\mathrm{ind}}^{(\mathrm{rs})}$, is calculated as the ensemble average of attenuation rates of individual wave elevations. The attenuation rate is defined as $Q_{\mathrm{ind}}^{(\mathrm{rs})} = \langle Q_i\rangle$, where Q_i is the attenuation rate extracted from the individual wave elevation $\eta = \eta_i$, i.e.

$$|\eta_i| \approx \mathrm{e}^{-Q_i x} \qquad (0 < x < L). \tag{3.9}$$

The interval length, L, the number of sub-intervals, M, and the size of the ensemble are chosen to be sufficiently large to capture attenuation rates accurately. In the numerical results presented in Section 5, we use intervals of length between 200 to 400 times the correlation length, l, four sub-intervals per correlation length and ensembles containing approximately 1000 samples.

3.2 *Bed profile*

We generate individual realisations of the bed profile, β, using a harmonic random process of the form

$$\beta(x) = \sqrt{\frac{2}{N}} \sum_{n=1}^{N} \cos\left(\kappa_n x + \varphi_n\right) \quad \text{where} \quad N \gg 1. \tag{3.10}$$

The frequencies κ_n and phases φ_n $(n = 1, \ldots, N)$ are both, respectively, identical and independently chosen random variables. The standard deviation of the bed profile, with respect to realisations, at all spatial locations x, is normalised to unity. Our approach is based on the derivation by Shinozuka [21], who showed the random process given in equation (3.10) is wide sense stationary, i.e. the probability density function, with respect to realisations, at any spatial point x is independent and identical Gaussian.

We prescribe probability density functions for frequencies κ_n and phases φ_n $(n = 1, \ldots, N)$ to satisfy the Gaussian autocorrelation condition (3.7). The phases are selected from a uniform distribution over the interval $[0, 2\pi)$. The frequencies are selected from a Gaussian distribution with zero mean and standard deviation equal to $\sqrt{2}/l$. The correct autocorrelation of the bed profiles is confirmed via the Wiener-Khinchin theorem and the central-limit theorem. In practice, we use $N = 100$ terms in the series expression for the bed profile, and confirm that the autocorrelation condition is satisfied numerically.

4. Multiple-scale approximation

We now consider an alternative method to capture the attenuation rate of the effective wave field. It provides an analytic expression for the attenuation rate. The method is based on the approach of Mei et al. [17], § 7.4. The problem considered differs, subtly, from the problem considered in Section 3, as the bed extends to infinity in both directions.

Begin by letting the correlation length, l, represent a local scale. We use the small non-dimensional quantity $\bar{k}\varepsilon$, which is also referred to as the non-dimensional bed amplitude, to define a complementary observation scale $l_2 = l/(\bar{k}\varepsilon)^2$, where $\bar{k}$ is the wavenumber for the mean fluid depth $\bar{h}$. The coordinates x and $x_2 = (\bar{k}\varepsilon)^2 x$ are used to define locations on the local and observation scales, respectively. We note that the attenuation rate does not vary on the intermediate scale, $l_1 = l/\bar{k}\varepsilon$. The corresponding coordinate, $x_1 = (\bar{k}\varepsilon)x$, is hence omitted.

We assume that the velocity potential can be expressed as

$$\phi(x, z) = \phi_0(x, x_2, z) + \bar{k}\varepsilon\phi_1(x, x_2, z) + (\bar{k}\varepsilon)^2\phi_2(x, x_2, z) + \mathrm{O}\left((\bar{k}\varepsilon)^3\right). \tag{4.1}$$

The multiple-scale expansion maps the velocity potential into the new coordinate system, and heuristically employs an asymptotic expansion in terms of the small quantity $\bar{k}\varepsilon$. The multiple-scale expansion is required so that the perturbation method is valid on both local and observation scales.

Governing equations for the functions ϕ_i $(i = 0, 1, 2)$ are derived by substituting the multiple-scale expansion (4.1) into the governing equations (2.2a–c), replacing horizontal derivatives ∂_x by $\partial_x + (\bar{k}\varepsilon)^2\partial_{x_2}$, and equating orders of $\bar{k}\varepsilon$. It is beneficial to begin by approximating the bed condition (2.2b) to order $(\bar{k}\varepsilon)^3$ by

$$\partial_z\phi = \bar{k}\varepsilon\frac{\partial_x(\beta\partial_x\phi)}{\bar{k}} + (\bar{k}\varepsilon)^2\frac{\partial_x(\beta^2\partial_{xz}\phi)}{2\bar{k}^2} \quad \text{on} \quad z = -\bar{h}. \tag{4.2}$$

We assume the derivatives of the bed profile are O(1).

4.1 *Order* 1

The governing equations for the leading-order term, ϕ_0, are

$$\partial_x^2\phi_0 + \partial_z^2\phi_0 = 0 \text{ in } \Omega_{\bar{h}}, \quad \partial_z\phi_0 = K\phi_0 \text{ on } z = 0 \quad \text{and} \quad \partial_z\phi_0 = 0 \text{ on } z = -\bar{h}. \tag{4.3}$$

The system is equivalent to that of a flat bed. Moreover, the system does not depend on the observation-scale coordinate explicitly.

We assume the leading-order solution consists of a modulated rightward-travelling wave (mimicking the incident wave used for a rough bed of finite length) and a random leftward-travelling wave (mimicking the reflected wave field for finite length roughness), i.e.

$$\phi_0(x, x_2, z) = \left(A(x_2)\mathrm{e}^{\mathrm{i}\bar{k}x} + B(x_2)\mathrm{e}^{-\mathrm{i}\bar{k}x}\right)\bar{w}(z) \quad \text{where} \quad \bar{w}(z) = \frac{\cosh\{\bar{k}(z+\bar{h})\}}{\cosh(\bar{k}\bar{h})}. \tag{4.4}$$

The amplitudes A and B are, as yet, unknown. They vary on the observation scale only. We emphasise the leading-order solution (4.4) fundamentally differs from that of Mei et al. [17], as (i) the rightward-travelling wave amplitude, A, contains a random (realisation-dependent) component, and (ii) the random leftward-travelling wave, with amplitude B, appears at leading order.

Fig. 2 provides evidence a left-travelling wave component should be included in the leading-order solution for long transects. The left-hand panel shows an individual wave elevation for non-dimensional bed amplitude $\bar{k}\varepsilon = 5 \times 10^{-2}$, correlation length $\bar{k}l = 0.75$ and bed depth $\bar{k}\bar{h} = 1$. The non-dimensional bed depth $\bar{k}\bar{h} = 1$, i.e. a mean water depth approximately one-sixth of the corresponding wavelength, is maintained for the numerical results presented from here on. The numerical method outlined in Section 3.1 is used to calculate the wave elevation. Therefore, the full wave elevations, η, are shown, rather than the leading-order solution, η_0.

The left-hand panel of Fig. 2 also shows rightward- and leftward-travelling components of the wave elevation, $\eta_+ = a_m\mathrm{e}^{\mathrm{i}k_m x}$ and $\eta_- = b_m\mathrm{e}^{-\mathrm{i}k_m x}$ $(x_{m-1} < x < x_m; m = 1, \ldots, M)$, respectively. The leftward-travelling component is greater than an $\mathrm{O}(\bar{k}\varepsilon)$ contribution to the wave elevation in a vicinity of the left-hand end of the interval containing the rough bed. It attenuates more rapidly than the rightward-travelling component, and therefore becomes $\mathrm{O}(\bar{k}\varepsilon)$ in a vicinity of the right-hand end of the interval.

The right-hand panel of Fig. 2 shows the ratio of the leftward- to rightward-travelling components as a function of scaled interval length. The ratio is represented via the quantity

$$H = \left\langle \frac{H_-}{H_+} \right\rangle \qquad \text{where} \qquad H_\pm = \frac{1}{L}\int_0^L |\eta_\pm| \, \mathrm{d}x, \tag{4.5}$$

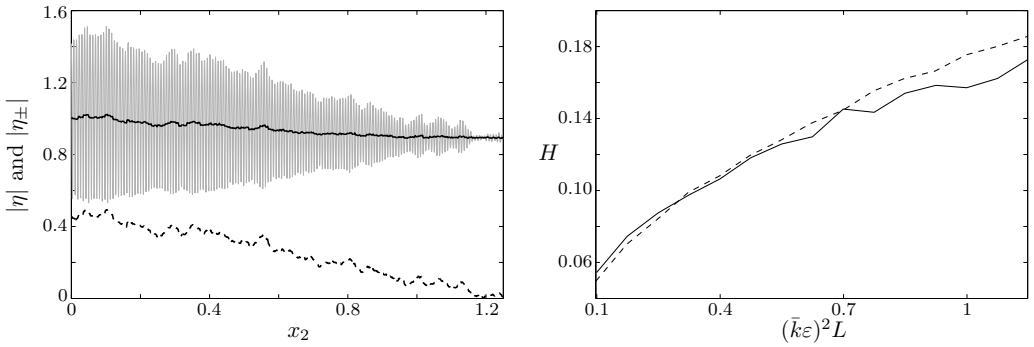

Fig. 2 Left-hand panel: individual wave elevation for non-dimensional bed amplitude $\bar{k}\varepsilon = 5 \times 10^{-2}$ and correlation length $\bar{k}l = 0.75$ (—), and split into rightward- and leftward-travelling components (— and --, respectively). Right-hand panel: mean ratio of leftward- to rightward-travelling components as a function of scaled interval length for non-dimensional bed amplitudes $\bar{k}\varepsilon = 5 \times 10^{-2}$ (—) and 10^{-1} (--), and correlation length $\bar{k}l = 0.75$.

i.e. the mean, with respect to simulations, of the ratio of the spatial means of the leftward- and rightward-travelling components. (An ensemble of wave elevations, calculated via the method outlined in Section 3.1, is used to approximate the mean with respect to realisations.) The quantity H does not, therefore, provide information on the variation of the ratio over the interval containing the rough bed. The ratio is shown for non-dimensional bed amplitudes $\bar{k}\varepsilon = 5 \times 10^{-2}$ and 10^{-1}, and correlation length $\bar{k}l = 0.75$. The two bed amplitudes produce almost identical results.

The ratio increases with interval length, as greater incident-wave energy is attenuated over longer intervals, which is balanced by a larger reflected-wave component. For an interval length equal to the observation scale, l_2, the magnitude of the leftward-travelling wave component is approximately 15 % of the magnitude of the rightward-travelling component.

The left-hand panel of Fig. 3 shows a second individual wave elevation for non-dimensional bed amplitude $\bar{k}\varepsilon = 5 \times 10^{-2}$ and correlation length $\bar{k}l = 0.75$. The wave elevation is decomposed into the effective wave elevation for the ensemble, $\langle\eta\rangle$, and its random component, $\eta - \langle\eta\rangle$. The random component is generally greater than an $\mathrm{O}(\bar{k}\varepsilon)$ contribution to the wave elevation.

The right-hand panel of Fig. 3 shows the magnitude of the random component of individual wave elevations as a function of non-dimensional correlation length, for non-dimensional bed amplitudes $\bar{k}\varepsilon = 10^{-3}$, 10^{-2} and 10^{-1}. The magnitude is represented via the quantity

$$I = \frac{1}{L}\int_0^L \langle|\eta(x) - \langle\eta(x)\rangle|\rangle \,\mathrm{d}x, \tag{4.6}$$

i.e. a spatial mean of the mean magnitude of the random component with respect to realisations. The interval length, L, is set to be 200 times the correlation length, and, with reference to the right-hand panel of Fig. 2, this is partially responsible for the increase in magnitude with increasing correlation length.

The right-hand panel of Fig. 3 shows the random component of the wave elevation is

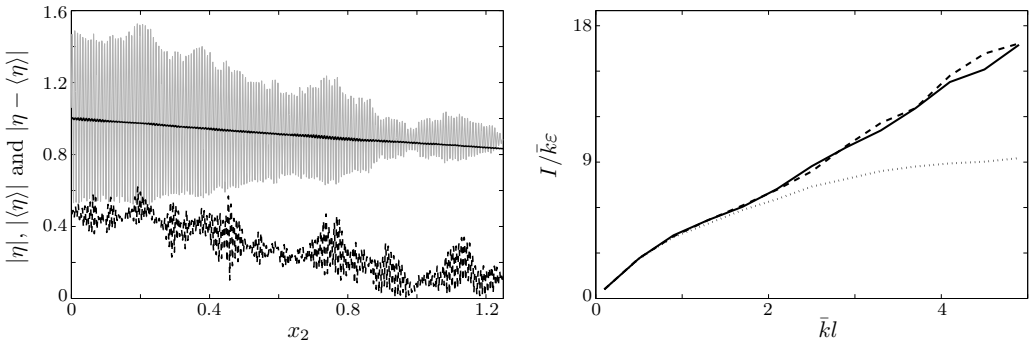

Fig. 3 Left-hand panel: individual wave elevation for non-dimensional bed amplitude $\bar{k}\varepsilon = 5{\times}10^{-2}$ and correlation length $\bar{k}l = 0.75$ (—), and split into effective and random components (— and - -, respectively). Right-hand panel: scaled magnitude of random component of wave elevation, as function of non-dimensional correlation length, for $\bar{k}\varepsilon = 10^{-3}$ (—), 10^{-2} (- -) and 10^{-1} ($\cdots$).

typically greater than an $\mathrm{O}(\bar{k}\varepsilon)$ contribution to individual wave elevations. It becomes the dominant contribution to the wave elevation as the correlation length increases. It is notable that the contribution of the random component scales with $\bar{k}\varepsilon$, until $\bar{k}\varepsilon = 10^{-1}$ and non-dimensional correlation lengths are approximately O(1) or greater.

4.2 *Order* $\bar{k}\varepsilon$

The governing equations for the term ϕ_1 are

$$\partial_x^2\phi_1 + \partial_z^2\phi_1 = 0 \qquad \text{in} \quad \Omega_{\bar{h}}, \tag{4.7a}$$

$$\partial_z\phi_1 = K\phi_1 \qquad \text{on} \quad z = 0 \tag{4.7b}$$

$$\text{and} \qquad \partial_z\phi_1 = \partial_x(\beta\partial_x\phi_0)/\bar{k} \quad \text{on} \quad z = -\bar{h}. \tag{4.7c}$$

The solution to the above problem is

$$\phi_1(x, x_2, z) = \int_{-\infty}^{\infty} G(|x - \check{x}|, z)\frac{\partial_{\check{x}}\{\beta(\check{x})\partial_{\check{x}}\phi_0(\check{x}, x_2, z)\}}{\bar{k}}\,\mathrm{d}\check{x}, \tag{4.8}$$

where G is the Green's function

$$G(x, z) = -\frac{1}{2\pi}\int_{\Gamma}\frac{\{\alpha\cosh(\alpha z) + K\sinh(\alpha z)\}\mathrm{e}^{\mathrm{i}\alpha(x-\check{x})}}{\alpha\{\alpha\sinh(\alpha\bar{h}) - K\cosh(\alpha\bar{h})\}}\,\mathrm{d}\alpha, \tag{4.9}$$

and Γ denotes the contour running along the real axis, but indented above the pole at $\alpha = -\bar{k}$ and below the pole at $\alpha = \bar{k}$.

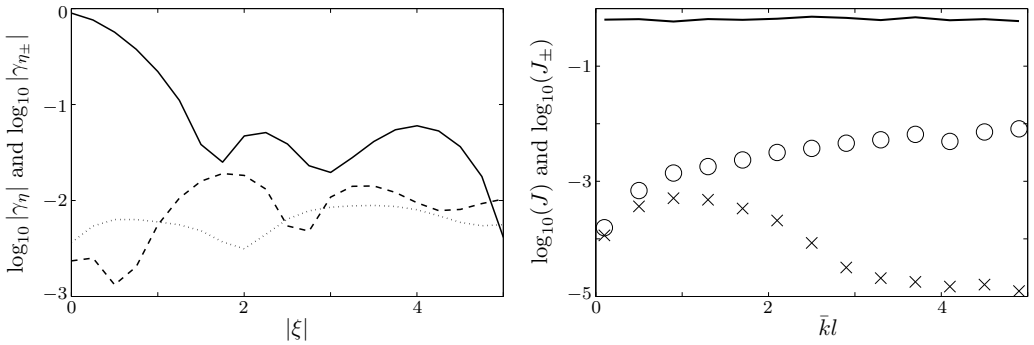

Fig. 4 Left-hand panel: correlation between wave elevations and bed profiles for non-dimensional bed amplitude $\bar{k}\varepsilon = 5 \times 10^{-2}$ and correlation length $\bar{k}l = 0.75$ (γ_η, —; γ_{η_+}, --; γ_{η_-}, $\cdots$). Right-hand panel: mean correlations of bed profile with wave elevation, J (—), and random components of wave elevation, J_+ ($\circ$) and J_- ($\times$), as functions of non-dimensional correlation length, for $\bar{k}\varepsilon = 10^{-2}$.

4.3 *Order* $(\bar{k}\varepsilon)^2$

Taking the ensemble average of the governing equations for ϕ_2, we obtain

$$\partial_x^2\langle\phi_2\rangle + \partial_z^2\langle\phi_2\rangle = -2\partial_{xx_2}\langle\phi_0\rangle \quad \text{in} \quad \Omega_{\bar{h}}, \tag{4.10a}$$

$$\partial_z\langle\phi_2\rangle = K\langle\phi_2\rangle \qquad \text{on} \quad z = 0 \tag{4.10b}$$

$$\text{and} \qquad \partial_z\langle\phi_2\rangle = \partial_x\langle\beta\partial_x\phi_1\rangle/\bar{k} \qquad \text{on} \quad z = -\bar{h}. \tag{4.10c}$$

We employ the ansatz $\langle\phi_2\rangle = \mathrm{e}^{\mathrm{i}\bar{k}x}F(x_2, z)$, which reduces equations (4.10a–b) to

$$\partial_z^2 F - \bar{k}^2 F = -2\mathrm{i}\bar{k}w\frac{\mathrm{d}\langle A\rangle}{\mathrm{d}x_2} \ \text{ for } \ -\bar{h} < z < 0 \quad \text{and} \quad \partial_z F = KF \ \text{ on } \ z = 0. \tag{4.11}$$

Similarly, the condition given in equation (4.10c) reduces to $\partial_z F = \mathcal{Q}$ on $z = -\bar{h}$, where

$$\mathcal{Q} = \frac{\mathrm{e}^{-\mathrm{i}\bar{k}x}}{\bar{k}^2}\,\partial_x\left\langle\beta(x)\partial_x\int_{-\infty}^{\infty} G(|x-\check{x}|, -\bar{h})\partial_{\check{x}}\{\beta(\check{x})\partial_{\check{x}}\phi_0(\check{x}, x_2, -\bar{h})\}\,\mathrm{d}\check{x}\right\rangle \tag{4.12a}$$

$$= \frac{\mathrm{e}^{-\mathrm{i}\bar{k}x}}{\bar{k}^2}\,\partial_x\int_{-\infty}^{\infty}\left(\partial_x G(|x-\check{x}|, -\bar{h})\right)\partial_{\check{x}}\left\langle\beta(x)\beta(\check{x})\partial_{\check{x}}\phi_0(\check{x}, x_2, -\bar{h})\right\rangle\,\mathrm{d}\check{x}. \tag{4.12b}$$

Fig. 4 provides evidence only the effective component of the leading-order solution contributes to the term $\left\langle\beta(x)\beta(\check{x})\partial_{\check{x}}\phi_0(\check{x}, x_2, -\bar{h})\right\rangle$ contained in the integrand of equation (4.12b). We use the wave elevation, η, as a proxy for the horizontal derivative of the velocity potential. The left-hand panel of Fig. 4 shows numerical approximations of the term

$$\gamma_\eta(|\xi|) = \langle\beta(x)\beta(\check{x})\eta(\check{x})\rangle = \langle\beta(\check{x}+\xi)\beta(\check{x})\eta(\check{x})\rangle, \tag{4.13}$$

as a function of $|\xi|$, where $\xi = x - \check{x}$, for non-dimensional bed amplitude $\bar{k}\varepsilon = 5 \times 10^{-2}$ and correlation length $\bar{k}l = 0.75$. (Pairs of points on a discrete mesh over the rough bed interval, $x \in (0, L)$, are used to calculate the correlation, i.e. all available x and ξ on the mesh.) The magnitude of the term γ_η approximates the Gaussian correlation specified for the bed profile (3.7). The left-hand panel also shows the random components of the terms, $\gamma_{\eta_\pm}$, where

$$\gamma_{\eta_+}(|\xi|) = \langle \beta(\check{x}+\xi)\beta(\check{x})(\eta_+(\check{x}) - \langle \eta(\check{x})\rangle)\rangle \quad \text{and} \quad \gamma_{\eta_-}(|\xi|) = \langle \beta(\check{x}+\xi)\beta(\check{x})\eta_-(\check{x})\rangle, \tag{4.14}$$

i.e. terms corresponding to the random component of the wave elevation travelling rightward, and the (random) wave elevation travelling leftward, respectively. The random components of the wave elevations are not correlated to the bed profile at leading order.

The right-hand panel of Fig. 4 provides evidence the random components of the wave elevation are uncorrelated to the bed profile for the range of correlation lengths considered in this investigation. Specifically, the panel shows numerical approximations of the mean magnitude of the terms $\gamma_{\eta_\pm}$ over the rough bed interval,

$$J_\pm = \frac{1}{L}\int_0^L |\gamma_{\eta_\pm}| \, \mathrm{d}\xi, \tag{4.15}$$

as functions of non-dimensional correlation length, for $\bar{k}\varepsilon = 10^{-2}$. For comparison, the panel also shows the mean magnitude of the term γ_η over one correlation length,

$$J = \frac{1}{l}\int_0^l |\gamma_\eta| \, \mathrm{d}\xi. \tag{4.16}$$

We therefore consider the random components of the leading-order term of the velocity potential, ϕ_0, to be uncorrelated to the bed profile, and eliminate the corresponding terms from the definition of $\mathcal{Q}$, to leave

$$\mathcal{Q} = \frac{\mathrm{e}^{-\mathrm{i}\bar{k}x}}{\bar{k}^2}\partial_x \left\langle \beta(x)\partial_x \int_{-\infty}^{\infty} G(|x-\check{x}|, -\bar{h})\partial_{\check{x}}\{\beta(\check{x})\partial_{\check{x}}\left(\langle A(x_2)\rangle \mathrm{e}^{\mathrm{i}\bar{k}\check{x}}\bar{w}(-\bar{h})\right)\} \, \mathrm{d}\check{x}\right\rangle. \tag{4.17}$$

Using the defined autocorrelation (3.7), the expression for $\mathcal{Q}$ is simplified to $\mathcal{Q} = \langle A(x_2)\rangle \mathcal{Q}_0$, where $\mathcal{Q}_0$ is the constant

$$\mathcal{Q}_0 = -\mathrm{sech}(\bar{k}\bar{h}) \int_{-\infty}^{\infty} G(|\xi|, -\bar{h}) \left\{ \left(\frac{\mathrm{d}}{\mathrm{d}\xi} - \mathrm{i}\bar{k}\right)^2 \gamma(\xi)\right\} \mathrm{e}^{-\mathrm{i}\bar{k}\xi} \, \mathrm{d}\xi. \tag{4.18}$$

Following Mei et al. [17], the governing equations for the unknown function F are now manipulated to produce an ordinary differential equation for the effective amplitude of the leading-order solution, $\langle A\rangle$, this being

$$\frac{\mathrm{d}\langle A(x_2)\rangle}{\mathrm{d}x_2} = \frac{-2\mathrm{i}\cosh(\bar{k}\bar{h})\mathcal{Q}_0\langle A(x_2)\rangle}{2\bar{k}\bar{h} + \sinh(2\bar{k}\bar{h})}. \tag{4.19}$$

The solution of the ordinary differential equation is

$$\langle A(x_2)\rangle = A_0 \exp\left(\frac{-2\mathrm{i}\cosh(\bar{k}\bar{h})\mathcal{Q}_0 x_2}{2\bar{k}\bar{h} + \sinh(2\bar{k}\bar{h})}\right), \tag{4.20}$$

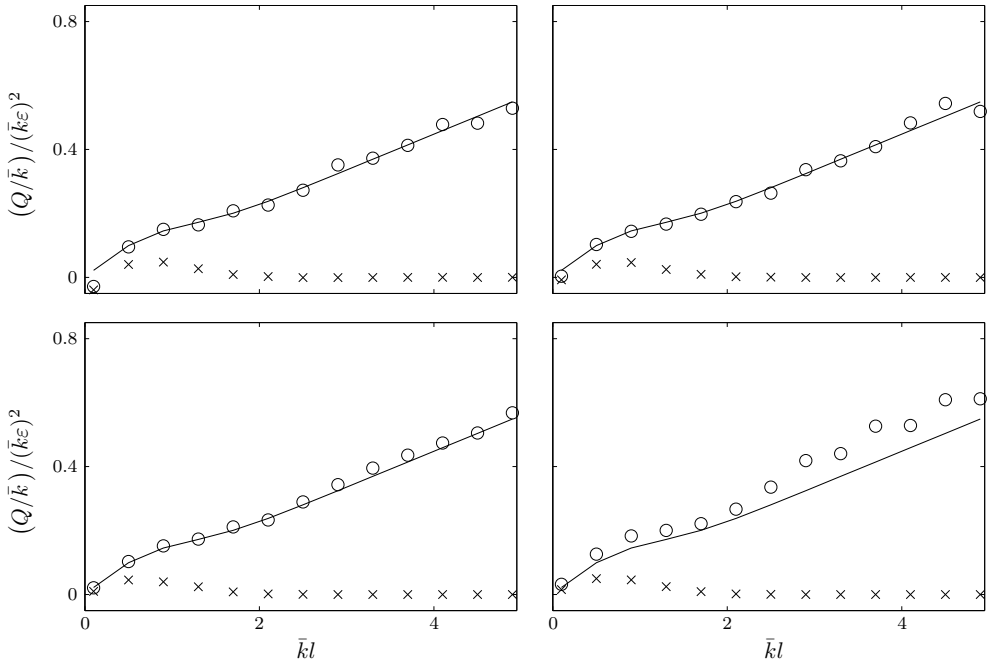

Fig. 5 Scaled attenuation rates, as functions of non-dimensional correlation length, predicted by the multiple-scale approximation (—, $Q_{\text{eff}}^{(\text{ms})}$), the numerical simulations of the effective wave field (∘, $Q_{\text{eff}}^{(\text{rs})}$) and the individual wave fields (×, $Q_{\text{ind}}^{(\text{rs})}$). Non-dimensional bed amplitude is $\bar{k}\varepsilon = 10^{-3}$ (top left-hand panel), 10^{-2} (top right), 10^{-1} (bottom left) and 2×10^{-1} (bottom right).

where A_0 is a constant. We deduce the attenuation rate of the leading-order effective wave field, as predicted by the multiple-scale approximation, to be

$$Q_{\text{eff}}^{(\text{ms})} = \frac{-2(\bar{k}\varepsilon)^2 \cosh(\bar{k}\bar{h})\text{Im}(\mathcal{Q}_0)}{2\bar{k}\bar{h} + \sinh(2\bar{k}\bar{h})} = \frac{2\sqrt{\pi}\bar{k}(\bar{k}\varepsilon)^2\bar{k}l(1 + \text{e}^{-(\bar{k}l)^2})}{\left(2\bar{k}\bar{h} + \sinh(2\bar{k}\bar{h})\right)^2}, \tag{4.21}$$

where the final expression results from manipulations outlined in Mei et al. [17]. Note that Mei et al. [17] assume the leading-order solution is deterministic, and hence equation (4.21) represents an attenuation rate for the envelope of the leading-order solution.

5. Numerical results

Fig. 5 shows attenuation rates predicted by the numerical simulations and multiple-scale approximation, scaled by $(\bar{k}\varepsilon)^2$, as functions of non-dimensional correlation length, for non-dimensional bed amplitudes $\bar{k}\varepsilon = 10^{-3}$, 10^{-2}, 10^{-1} and 2×10^{-1}. The multiple-scale approximation (4.21) is proportional to $(\bar{k}\varepsilon)^2$, and thus the corresponding scaled attenuation rate is independent of the non-dimensional bed amplitude.

The numerical approximation of attenuation rates of the effective wave elevations agree

with the corresponding multiple-scale approximations for the three smaller values of non-dimensional bed amplitude, $\bar{k}\varepsilon = 10^{-3}$, 10^{-2} and 10^{-1}. (The small difference between the two approximations for the smallest correlation length and bed amplitude is attributed to numerical difficulty in capturing very small attenuation rates accurately.) The agreement confirms accuracy of the multiple-scale approximation for small-amplitude roughness. It follows that in the small-amplitude regime, $\bar{k}\varepsilon \leqslant 10^{-1}$, the effective attenuation rate is proportional to the square of the bed amplitude.

For the largest non-dimensional bed amplitude, $\bar{k}\varepsilon = 2 \times 10^{-1}$, the attenuation rates of the effective wave elevations predicted by the numerical simulations slightly exceed those predicted by the multiple-scale approximation. The results therefore indicate the limit of validity of the multiple-scale approximation.

The attenuation rates of the individual wave elevations, as predicted by the numerical simulations, have qualitative and quantitative properties markedly different from those of the effective wave elevations. The qualitative behaviour of the attenuation rate of individual wave elevations is intuitive. The attenuation rate is approximately zero (on the linear scale shown) for the smallest non-dimensional correlation length considered, $\bar{k}l = 0.1$. In this regime, the random bed fluctuations are too rapid to be seen by the waves. The attenuation rate is also approximately zero for correlation lengths greater than two. The roughness in this regime is too mild to modulate the waves. The attenuation rate is only non-zero for correlation lengths between these two regimes, where the roughness is long enough to be seen by the waves and short enough to modulate the waves.

The largest attenuation rate of the individual wave elevations is $Q_{\mathrm{ind}}^{(\mathrm{rs})}/\bar{k} \approx 0.05(\bar{k}\varepsilon)^2$ for $\bar{k}\varepsilon = 10^{-1}$. It corresponds to a localisation length, i.e. factor e^{-1} reduction in wave amplitude, of approximately 320 wavelengths. However, attenuation rates of the individual wave elevations are typically much smaller. For example, for correlation lengths greater than two $Q_{\mathrm{ind}}^{(\mathrm{rs})}/\bar{k} \approx \mathrm{O}(10^{-4}) \times (\bar{k}\varepsilon)^2$. For $\bar{k}\varepsilon = 10^{-2}$ this corresponds to a localisation length of $\mathrm{O}(10^7)$ wavelengths.

Attenuation of the effective wave elevation is therefore not indicative of attenuation of individual wave elevations. Although the rough seabed forces a random component of the individual wave elevations, as shown in the left-hand panel of Fig. 3, the individual wave elevations do not attenuate. We deduce that the dominant source of attenuation of the effective wave elevation is wave cancellation, i.e. decoherence.

Fig. 6 supports the above conclusion. It shows example individual wave elevations and corresponding effective wave elevations, for a non-dimensional bed amplitude $\bar{k}\varepsilon = 10^{-2}$, and correlation lengths $\bar{k}l = 0.9$ and 5. The smaller correlation length, $\bar{k}l = 0.9$, is chosen to produce visible (although weak) attenuation of the individual wave elevation. The corresponding effective wave elevation attenuates slightly more rapidly than the individual wave elevation.

The largest correlation length, $\bar{k}l = 5$, is chosen to produce maximal attenuation of the effective wave elevation. The corresponding individual elevation does not attenuate (on the scale shown). Attenuation of the effective elevation is therefore not related to the individual elevations.

Fig. 7 shows the scaled attenuation rates, as functions of non-dimensional bed amplitude, for correlation length $\bar{k}l = 1$, i.e. a correlation length that produces attenuation of the individual wave elevations. The results confirm the multiple-scale approximation

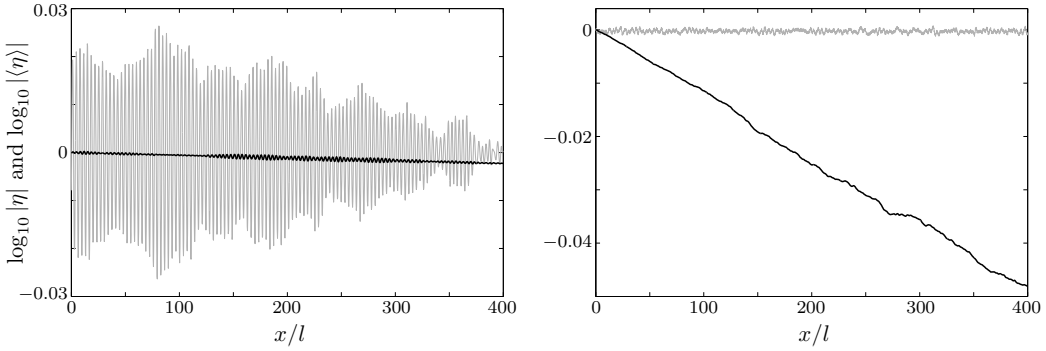

Fig. 6 Example individual wave elevations (grey curves) and corresponding effective wave elevations (black), for non-dimensional bed amplitude $\bar{k}\varepsilon = 10^{-2}$ and correlation length $\bar{k}l = 0.9$ (left-hand panel) and 5 (right).

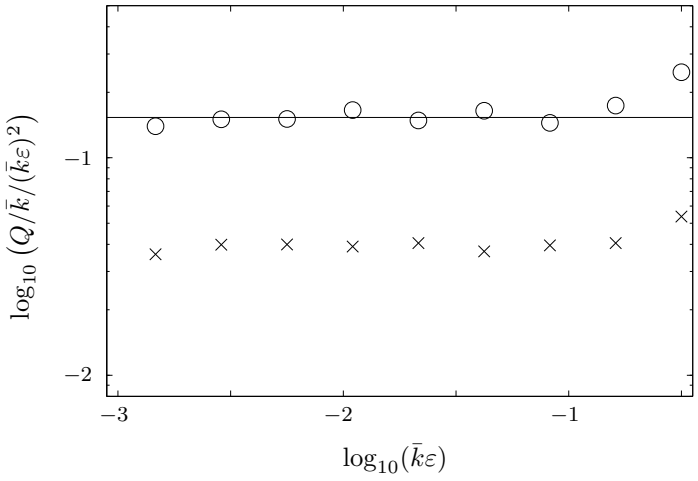

Fig. 7 Attenuation rates as functions of non-dimensional bed amplitude, for non-dimensional correlation length $\bar{k}l = 1$. Curve/marker labels follow those used in Fig. 5.

captures the attenuation rate of the effective elevation for non-dimensional bed amplitudes smaller than approximately $\bar{k}\varepsilon = 10^{-1}$. The results clearly display the multiple-scale approximation's loss of accuracy, and under-prediction of the effective attenuation rate, for bed amplitudes greater than 10^{-1}.

Fig. 7 also indicates the attenuation rates of the individual wave elevations and effective elevation share the same qualitative properties, as functions of bed amplitude. In particular, attenuation rates are proportional to the bed amplitude squared, for non-dimensional bed amplitudes less than 10^{-1}. Further, the attenuation rates increase with increasing bed amplitudes more rapidly than the bed amplitude square for non-dimensional bed amplitudes larger than 10^{-1}.

6. Summary and discussion

Numerical simulations of small-amplitude ocean waves propagating over a rough seabed in intermediate water depth have been used to reappraise the possibility of the roughness causing localisation of the waves, as predicted by Mei and Hancock [12] and Mei et al. [17] using a multiple-scale approximation. We focussed on the viability of using the effective, i.e. mean, wave field to predict attenuation, and hence localisation.

Numerical results were used to show that for small-amplitude roughness, the attenuation rate of the effective wave elevation scales with the square of the roughness amplitude. Further, it was shown that the attenuation rate of the effective wave elevation can be captured analytically via the multiple-scale approximation.

However, individual wave elevations attenuate at a far slower rate than the effective wave elevation. In most cases attenuation rates of individual wave elevations are too small for wave localisation to be realised in the ocean.

It was deduced that the effective wave elevation attenuates due to wave cancellation in the averaging process. The attenuated wave energy is transferred to the random components of the individual wave fields. The multiple-scale approximation used does not give information about the random components. Use of the effective wave elevation, therefore, results in misleading predictions of localisation.

A single-mode approximation was applied as part of the numerical procedure. The approximation reduces the governing equations for water waves over a rough seabed to the steady-state one-dimensional wave equation with a varying wave number. The finding that individual wave fields attenuate far slower through a rough medium than the corresponding effective wave field is, therefore, expected to hold in general for linear one-dimensional waves in the analogous scaling regime for the physical context under consideration.

We thank Dirk Blömker for helpful discussions and Fabien Montiel for highlighting the work of Wu [18] to us. This work was supported by the Group of Eight, Australia, and German Academic Exchange Service (DAAD) Joint Research Co-operation Scheme. LB acknowledges funding support from the Australian Research Council (DE130101571) and the Australian Antarctic Science Grant Program (Project 4123). The eResearch South Australia computing facility was used to perform numerical simulations.

References

[1] M. Belzons, E. Guazzelli, and O. Parodi. Gravity waves on a rough bottom: experimental evidence of one-dimensional localization. *J. Fluid Mech.*, 186:539558, 1988.

[2] P. Devillard, F. Dunlop, and B. Souillard. Localization of gravity waves on a channel with a random bottom. *J. Fluid Mech.*, 186:521538, 1988.

[3] E. Guazzelli, E. Guyon, and B. Soulliard. On the localisation of shallow water waves by a random bottom. *J. Phys. Paris*, 44:L837841, 1983.

[4] A. Nachbin and G. C. Papanicolaou. Water waves in shallow channels of rapidly varying depth. *J. Fluid Mech.*, 241:311332, 1992.

[5] A. Nachbin. The localization length of randomly scattered water waves. *J. Fluid Mech.*, 296:353372, 1995.

[6] A. Nachbin and K. Sølna. Apparent diffusion due to topographic microstructure in shallow waters. *Phys. Fluids*, 15(1):6677, 2003.

[7] G. Grataloup and C. C. Mei. Long waves in shallow water over a random seabed. *Phys. Rev. E*, 68:026314, 2003.

[8] C. C. Mei and Y. Li. Evolution of solitons over a randomly rough seabed. *Phys. Rev. E*, 70:016302, 2004.

[9] W. Craig, P. Guyenne, and C. Sulem. Water waves over a random bottom. *J. Fluid Mech.*, 640:79107, 2009.

[10] E. Pelinovsky, A. V. Razin, and E. V. Sasorova. Berkhoff approximation in a problem on surface gravity wave propagation in a basin with bottom irregularities. *Waves Random Complex Media*, 8(2):255268, 1998.

[11] A. Stepaniants. Diffusion and localisation of surface gravity waves over irregular bathymetry. *Phys. Rev. E*, 63:031202, 2001.

[12] C. C. Mei and M. J. Hancock. Weakly nonlinear surface waves over a random bed. *J. Fluid Mech.*, 475:247268, 2003.

[13] T. Kawahara. Effect of random inhomogeneities on nonlinear propagation of water waves. *J. Phys. Soc. Japan*, 41(4):14021409, 1976.

[14] J. H. Pihl, C. C. Mei, and M. J. Hancock. Surface gravity waves over a two-dimensional random sea bed. *Phys. Rev. E*, 66:016611, 2002.

[15] A. M. Luz and A. Nachbin. Wave packet defocusing due to a highly disordered bathymetry. *Stud. Appl. Math.*, 130(4):393416, 2013.

[16] Y. Li and C. C. Mei. Scattering of internal tides by irregular bathymetry of large extent. *J. Fluid Mech.*, 747:481505, 2014.

[17] C. C. Mei, M. Stiassnie, and D. K.-P. Yue. *Theory and applications of ocean surface waves. Part I: linear aspects.* World Scientific, 2005.

[18] R. Wu. Mean field attenuation and amplitude attenuation due to wave scattering. *Wave Motion*, 4:305–316, 1982.

[19] S. A. Shapiro and G. Kneib. Seismic attenuation by scattering: Theory and numerical results. *Geophys. J. Int.*, 114:373–391, 1993.

[20] L. G. Bennetts and V. A. Squire. Wave scattering by multiple rows of circular ice floes. *J. Fluid Mech.*, 639:213–238, 2009.

[21] M. Shinozuka. Simulation of multivariate and multidimensional random processes. *J. Acoust. Soc. Am.*, 49(1):357368, 1971.